
Critic Regularized Regression

Ziyu Wang*[†]
ziyu@google.com

Alexander Novikov*
anovikov@google.com

Konrad Żółna*
kondiz@google.com

Jost Tobias Springenberg*
springenberg@google.com

Scott Reed*
reedscot@google.com

Bobak Shahriari*
bshahr@google.com

Noah Siegel*
siegeln@google.com

Josh Merel*
jsmerel@google.com

Caglar Gulcehre*
caglarg@google.com

Nicolas Heess*
heess@google.com

Nando de Freitas*
nando@google.com

Abstract

Offline reinforcement learning (RL), also known as batch RL, offers the prospect of policy optimization from large pre-recorded datasets without online environment interaction. It addresses challenges with regard to the cost of data collection and safety, both of which are particularly pertinent to real-world applications of RL. Unfortunately, most off-policy algorithms perform poorly when learning from a fixed dataset. In this paper, we propose a novel offline RL algorithm to learn policies from data using a form of critic-regularized regression (CRR). We find that CRR performs surprisingly well and scales to tasks with high-dimensional state and action spaces – outperforming several state-of-the-art offline RL algorithms by a significant margin on a wide range of benchmark tasks.

1 Introduction

Deep reinforcement learning (RL) algorithms have succeeded in a number of challenging domains. However, few of these domains have involved real-world decision making. One important reason is that online execution of policies during learning, which we refer to as *online RL*, is often not feasible or desirable because of cost, safety and ethics [8]. This is clearly the case in healthcare, industrial control and robotics. Nevertheless, for many of these domains, large amounts of historical data are available. This has led to a resurgence of interest in *offline RL* methods, also known as batch RL [19], which aim to learn policies from logged data without further interaction with the real system.

This interest in offline RL is further amplified by the evaluation crisis in RL: RL involves a close interplay between exploration and learning from experiences, which makes it difficult to compare algorithms. By decoupling these two problems and focusing on learning from fixed experiences, it becomes possible to share datasets with benchmarks to improve collaboration and evaluation in the field.

The naive application of off-policy RL algorithms with function approximation to the offline setting has often failed, and has prompted several alternative solutions [e.g. 9, 17, 30]. A shared conclusion is that failure stems from overly optimistic Q-estimates, as well as inappropriate extrapolation beyond

*DeepMind, London, United Kingdom.

[†]Google Brain, Toronto, Canada.

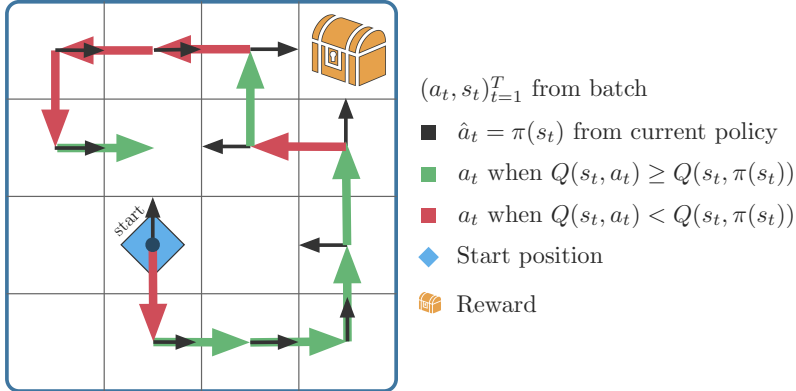


Figure 1: Illustration of the main idea behind CRR. The task is to reach the reward from the starting position as fast as possible. Consider learning a policy from the suboptimal (red/green) trajectory. For every state s_t , the action proposed by the current (suboptimal) policy $\pi(s_t)$ is shown with black arrows. CRR compares the critic prediction of the value $Q(s_t, a_t)$ of the action a_t from the trajectory against the value $Q(s_t, \pi(s_t))$ of the action from the policy π . If $Q(s_t, a_t) \geq Q(s_t, \pi(s_t))$, the corresponding action is marked green and the pair (s_t, a_t) is used to train the policy. If $Q(s_t, a_t) < Q(s_t, \pi(s_t))$, the action is marked red and is not used to train the policy. Thus, CRR filters out bad actions and enables learning better policies from low-quality data.

the observed data. This is especially problematic in combination with bootstrapping, where the Q-function is queried for actions that were not observed, and where errors can accumulate.

In this paper, we propose a novel offline RL algorithm to learn policies from data using a form of *critic-regularized regression* (CRR). CRR essentially reduces offline policy optimization to a form of value-filtered regression that requires minimal algorithmic changes to standard actor-critic methods. It is therefore easy to understand and implement. Figure 1 provides an intuitive explanation of CRR.

Despite the apparent simplicity of CRR, our experiments show that it outperforms several state-of-the-art offline RL algorithms by a significant margin on a wide range of benchmark tasks. Moreover, and very importantly, it scales to tasks with high-dimensional state and action spaces, and does well on datasets of diverse or low-quality data.

2 Related Work

For comprehensive in-depth reviews of offline RL, we refer the reader to Lange et al. [19] and Levine et al. [20]. The latter provides an extensive and very recent appraisal of the field.

Behavior cloning (BC) [28] is the simplest form of offline learning. Starting from a dataset of state-action pairs, a policy is trained to map states to actions via a supervised loss. This approach can be surprisingly effective when the dataset contains high-quality data, e.g. trajectories generated by an expert for the task of interest; see Merel et al. [22] for a large scale application. However, it can easily fail (i) when the dataset contains a large proportion of random or otherwise task irrelevant behavior; or (ii) when the learned policy induces a trajectory distribution that deviates far from that of the dataset under consideration [29].

Off-policy deep RL algorithms provide an alternative to BC. Unlike BC, these methods can take advantage of reward functions to outperform the demonstrator, see e.g. Cabi et al. [6]. Recently, it was shown that distributional off-policy deep RL techniques [5, 4], unlike their non-distributional counterparts, work well for offline RL in Atari [2] and robot manipulation [6]. A recent paper by Fujimoto et al. [9] has corroborated that distributional variants by themselves can be more effective, but under-perform in comparison to an algorithm purposely designed for offline RL, known as Batch-Constrained deep Q-learning (BCQ) [10].

Several methods have been proposed to overcome problems with off-policy deep RL in the offline setting. These failures have mostly been attributed to inappropriate generalization and overly confident Q estimates. One line of work focused on constraining the action choices to the support of the training data [10, 17, 30, 15]. This can be achieved by first learning a generative model of the data, and then sampling actions from this model for Q-learning [10]. The generative model can also be used with

constrained optimization to restrict the estimated RL policy [17, 15]. Both Fujimoto et al. [10] and Kumar et al. [17] further employ multiple Q-function estimates to reduce the optimism bias.

A second line of attack in offline RL has been to perform weighted behavior cloning. The idea is to use an estimate of the advantage function to select the best actions in the dataset for BC. This is similar in spirit to the motivation provided in Figure 1. Examples of this approach include monotonic advantage re-weighted imitation learning (MARWIL) [37], best-action imitation learning (BAIL) [7], advantage-weighted behavior models (ABM) [30] and advantage weighted regression [27], which has previously been studied in the form of a Fitted Q-iteration algorithm with low-dimensional policy classes [26]. Our approach differs from most of these in that we do not rely on observed returns for advantage estimation – as elaborated on in Sec. 3. Additionally, we introduce a technique we call Critic Weighted Policy (CWP) that uses the learned critic to improve results at test time.

A simple (binary) version of the filtering component of CRR was proposed by Nair et al. [25], whose results showed that the filter simply accelerated training, but gave mixed results in long horizons. An earlier version of a similar algorithm can be found in van Hasselt and Wiering [36]. It is important to note that these works perform filtered BC but in online settings, in which further data collection is allowed, and hence filtering may play a lesser role. The online setting is considerably more forgiving than the offline setting, which is the focus of this paper. Indeed, our analysis in Section 4 demonstrates that in the offline setting, design elements such as sample estimates for binary and exponential filtering, policy improvement with CWP, carefully designed deep recurrent networks, and the use of distributional value functions make a dramatic difference in the quality of the results.

3 Critic Regularized Regression

We derive Critic Regularized Regression (CRR), a simple, yet effective, method for offline RL.

3.1 Policy Evaluation

Suppose we are given a fixed dataset \mathcal{B} containing either individual transition tuples $(\mathbf{s}_t, \mathbf{a}_t, r_t, \mathbf{s}_{t+1})$ or K -step trajectories $(\mathbf{s}_t, \mathbf{a}_t, r_t, \mathbf{s}_{t+1}, \mathbf{a}_{t+1}, \dots, \mathbf{s}_{t+K})$. For brevity we will consider only the first case, but all algorithmic developments directly apply for K -step trajectories. An important step in many off-policy learning approaches is off-policy policy evaluation. This often involves learning an approximation to the Q-function minimizing a temporal difference loss similar to the following

$$\mathbb{E}_{\mathcal{B}} \left[D \left(Q_{\theta}(\mathbf{s}_t, \mathbf{a}_t), (r_t + \gamma \mathbb{E}_{\mathbf{a} \sim \pi(\mathbf{s}_{t+1})} Q_{\theta'}(\mathbf{s}_{t+1}, \mathbf{a})) \right) \right], \quad (1)$$

where the expectation over data is approximated by sampling $(\mathbf{s}_t, \mathbf{a}_t, r_t, \mathbf{s}_{t+1}) \sim \mathcal{B}$ and D is some divergence measure; measuring discrepancy between the current estimate of the action-value $Q_{\theta}(\mathbf{s}_t, \mathbf{a}_t)$ (for policy π) and the td-update, based on a target network [24]. We note that we make use of a distributional Q-function as in Barth-Maroon et al. [4], instead of using a squared error for D .

As discussed in recent work, [e.g. 10, 17, 30], without environment interaction (the offline RL setting) this loss may be problematic due to the “bootstrapping” issue mentioned above; where we evaluate the value of the next state \mathbf{s}_{t+1} by $\mathbb{E}_{\mathbf{a} \sim \pi(\mathbf{s}_{t+1})} Q_{\theta'}(\mathbf{s}_{t+1}, \mathbf{a})$. If trained with standard RL, a parametric $\pi(\cdot | \mathbf{s}_{t+1})$ is likely to extrapolate beyond the training data and to propose actions that are not contained in \mathcal{B} . For these actions Q will not have been trained and may produce bad estimates.

3.2 Policy Learning with CRR

To mitigate the aforementioned problem, we want to avoid evaluating Q for $(\mathbf{s}, \mathbf{a}) \notin \mathcal{B}$. Thus, we aim to train π by discouraging it from taking actions that are outside the training distribution. Such a requirement would be hard to achieve with standard policy gradients [e.g. 31, 12, 33]. We thus change our objective to match the state-action mapping contained in the training data – but filtered by the Q-function. Specifically, we optimize

$$\arg \max_{\pi} \mathbb{E}_{(\mathbf{s}, \mathbf{a}) \sim \mathcal{B}} \left[f(Q_{\theta}, \pi, \mathbf{s}, \mathbf{a}) \log \pi(\mathbf{a} | \mathbf{s}) \right], \quad (2)$$

where f is a non-negative, scalar, function whose value is monotonically increasing in Q_{θ} . Fundamentally, Eq. (2) tries to copy actions that exist in the data, thereby restricting π . Further properties

Algorithm 1: Critic Regularized Regression

Input: Dataset \mathcal{B} , critic net Q_θ , actor net π_ϕ , target actor and critic nets: $\pi_{\phi'}$, $Q_{\theta'}$, function f
for $n_{updates}$ **do**
 Sample $(\mathbf{s}_t^i, \mathbf{a}_t^i, r_t^i, \mathbf{s}_{t+1}^i)_{i=1}^b$ from \mathcal{B} .
 Update actor (policy) with gradient: $\nabla_\phi - \frac{1}{b} \sum_i \log \pi_\phi(\mathbf{a}_t^i | \mathbf{s}_t^i) f(Q_\theta, \pi_\phi, \mathbf{s}_t^i, \mathbf{a}_t^i)$
 Update critic with gradient: $\nabla_\theta \frac{1}{b} \sum_i D[Q_\theta(\mathbf{s}_t^i, \mathbf{a}_t^i), (r_t^i + \gamma \mathbb{E}_{\mathbf{a} \sim \pi_{\phi'}(\mathbf{s}_{t+1}^i)} Q_{\theta'}(\mathbf{s}_{t+1}^i, \mathbf{a}))]$
 Update the target actor/critic nets every N steps by copying parameters: $\theta' \leftarrow \theta$, $\phi' \leftarrow \phi$.
end

of the learning objective can be controlled through different choices of f , for example when $f := \mathbb{1}$, Eq. (2) is equivalent to Behavioral Cloning (BC). The success of BC is, however, highly dependent on the quality of the dataset \mathcal{B} . When \mathcal{B} does not contain enough transitions generated by a policy performing well on the task, or the fraction of poor data is too large, then BC is likely to fail.

Provided Q is sufficiently accurate for $(\mathbf{s}, \mathbf{a}) \in \mathcal{B}$ (e.g. learned using Eq. (1)), we can consider additional choices of f that enable off-policy learning to overcome this problem:

$$f := \mathbb{1}[\hat{A}_\theta(\mathbf{s}, \mathbf{a}) > 0], \quad (3)$$

$$f := \exp\left(\hat{A}_\theta(\mathbf{s}, \mathbf{a})/\beta\right), \quad (4)$$

where $\beta > 0$ is a hyper-parameter, $\mathbb{1}$ the indicator function, and $\hat{A}_\theta(\mathbf{s}, \mathbf{a})$ is an estimated advantage function. Eq. (2) bears similarity to the objective for training the behavior prior in [30]. More precisely, by using f from Eq. (3) and \hat{A}_K (see Table 1) we recover the form of the ABM ‘prior-policy’. Intuitively, Eq. (3) entails BC on a filtered dataset where the filtering increases the average quality of the actions we learn from. The filter is defined in terms of the value of the current policy.

Exponential weighting as regularized policy iteration. We can gain insight into Eq. (4) by realizing that it approximately implements a regularized policy improvement step in a policy iteration scheme. Consider

$$\mathcal{L}(q, \mu_{\mathcal{B}}) = \mathbb{E}_{\mathbf{s} \sim \mathcal{B}} \left[\mathbb{E}_q [Q_\theta(\mathbf{s}, \mathbf{a})] + \beta \text{KL}[q(\cdot | \mathbf{s}), \mu_{\mathcal{B}}(\cdot | \mathbf{s})] \right], \quad (5)$$

where $\mu_{\mathcal{B}}$ is the policy that generated the data. This objective is similar to the off-policy improvement from MPO [1] – but with $\mu_{\mathcal{B}}$ instead of the policy prior. The optimal policy for this objective can be written as $q(\mathbf{a} | \mathbf{s}) = \frac{\exp(Q_\theta(\mathbf{s}, \mathbf{a})/\beta) \mu_{\mathcal{B}}(\mathbf{a} | \mathbf{s})}{Z(\mathbf{s})}$. $Z(\mathbf{s})$ is hard to evaluate in our setting (we only have access to \mathcal{B}) so we use $q(\mathbf{a} | \mathbf{s}) \propto \exp(\hat{A}_\theta(\mathbf{s}, \mathbf{a})/\beta)$ in practice, thus performing an implicit, approximate per state normalization by subtracting $V(\mathbf{s})$. Projecting this distribution back onto the parametric policy π_ϕ can be done by minimizing the cross-entropy $H[q(\cdot | \mathbf{s}), \pi_\phi(\cdot | \mathbf{s})]$. Again, to avoid computing the normalizing constant for q , we use samples from the dataset \mathcal{B} to estimate this cross-entropy, which yields Eq. (2) with f chosen as in Eq. (4). Minimizing this cross-entropy corresponds to “sharpening” the action distribution $\mu_{\mathcal{B}}$, giving higher weight to better actions. Further, as $\beta \rightarrow \infty$ this objective becomes behavior cloning (BC).

Theoretical analysis in the tabular setting. In the Appendix, we show that in the tabular setting, CRR is safe in the sense that it restricts the action choice to the support of the data, and can be interpreted as implementing a policy iteration scheme that improves upon the behavior policy.

On the choice of advantage estimators. Since we are interested in high-dimensional action spaces, we use a sample estimate of the advantage in CRR (Algorithm 1). We contrast different choices for \hat{A} in Table 1. From these we consider \hat{A}_{mean} but found that for small m it may overestimate the advantage due to stochasticity. For f as in Eq. (3) this could lead to sub-optimal actions being included. We therefore also consider \hat{A}_{max} ; a pessimistic estimate of the advantage.

Except for the work on FQI-AWR [26] – where the authors considered a simpler setting, learning both Q and V with simple kernel based regression followed by policy learning based on advantage weighting – the recent literature has mainly considered K -step or Monte-Carlo return based estimates of the advantage (\hat{A}_K, \hat{A}_{MC} in the table). Among these, our formulation in Eq. (3) and Eq. (4) is similar to [30] as highlighted above. It also bears some similarity to recent work on advantage weighted regression [37, 27], which uses \hat{A}_K , or \hat{A}_{MC} with a learned V -function to form advantage

Table 1: Advantage estimates considered by different algorithms.

Advantage estimate	Algorithms
$\hat{A}_{\text{mean}}(\mathbf{s}_t, \mathbf{a}_t) = Q_{\theta}(\mathbf{s}_t, \mathbf{a}_t) - \frac{1}{m} \sum_{j=1}^m Q_{\theta}(\mathbf{s}_t, \mathbf{a}^j)$, with $\mathbf{a}^j \sim \pi(\cdot \mathbf{s}_t)$	CRR, FQI-AWR[26]
$\hat{A}_{\text{max}}(\mathbf{s}_t, \mathbf{a}_t) = Q_{\theta}(\mathbf{s}_t, \mathbf{a}_t) - \max_{j=1}^m Q_{\theta}(\mathbf{s}_t, \mathbf{a}^j)$, with $\mathbf{a}^j \sim \pi(\cdot \mathbf{s}_t)$	CRR(max)
$\hat{A}_k(\mathbf{s}_t, \mathbf{a}_t) = \gamma^K V(\mathbf{s}_{t+K}) + \sum_{t'=t}^{t+K-1} \gamma^{t'-t} r(\mathbf{s}_{t'}, \mathbf{a}_{t'}) - V(\mathbf{s}_t)$	ABM[30]
$\hat{A}_{MC}(\mathbf{s}_t, \mathbf{a}_t) = \sum_{t'=t}^{\infty} \gamma^{t'-t} r(\mathbf{s}_{t'}, \mathbf{a}_{t'}) - V(\mathbf{s}_t)$	MARWIL[37], AWR[27]

estimates. A choice that we find to not work well in many offline RL scenarios, as we explain below. A full listing of our algorithm is given in 1; where we also adopt standard practices from the deep RL literature to stabilize training (e.g. target networks) and note that we use a distributional critic.

CRR vs. return-based methods. Using K-step returns (with $K > 1$) can be problematic when the data is very off-policy as we will show experimentally in the appendix. Additionally, in stochastic environments, using K-step (or episodic) returns for estimating advantages may lead to risk seeking or otherwise undesirable behavior. To illustrate this point, let us consider the following simple two-armed bandit problem: the first arm generates a payoff of either 0, or 1 with 50% probability each. The second arm generates a deterministic payoff of 0.9 – it hence should be the favored arm. Let us assume that 2/3 of the actions in our data-set pull the first arm and the remaining 1/3 the second arm. A perfectly learned Q function would clearly favor arm two over arm one. By using returns R for advantage estimation (computing advantages as $R - V$), however, Advantage weighted regression (AWR) [27], or similar methods, would favor the first arm over the second arm; regardless of the temperature parameter. Similarly, the prior learned in ABM [30] would choose the two actions equally and therefore also fall short. For ABM, the additional RL step could potentially recover the correct action choice (depending on how far the RL policy is allowed to deviate from the prior) but no guarantee exists that it will. Last but not least, methods that rely on reward filtering would also favor arm one over arm two [7, 18].

Critic Weighted Policy (CWP). The learned Q -function can be used during policy execution to perform an additional approximate policy improvement step. Indeed, search-based methods have made use of this fact in discrete domains [32]. We can consider the solution of Eqn. (5) albeit now using the learned policy π_{ϕ} as the prior. The solution is given by $\bar{q} = \arg \max_{\bar{q}} \mathcal{L}(\bar{q}, \pi_{\phi})$, which yields $\bar{q}(\mathbf{a} | \mathbf{s}) = \frac{\exp(Q_{\theta}(\mathbf{s}, \mathbf{a}) / \beta) \pi_{\phi}(\mathbf{a} | \mathbf{s})}{Z(\mathbf{s})}$. We can use this policy instead of π during action selection. To sample from \bar{q} , we use importance sampling. We first sample actions $\mathbf{a}_{1:n}$ from $\pi_{\phi}(\cdot | \mathbf{s})$, weight the different actions by their importance weights $\exp(Q_{\theta}(\mathbf{s}, \mathbf{a}_i) / \beta)$ and finally choose an action by re-sampling with probabilities $P(\mathbf{a}_i) = \frac{\exp(Q_{\theta}(\mathbf{s}, \mathbf{a}_i) / \beta)}{\sum_{j=1}^n \exp(Q_{\theta}(\mathbf{s}, \mathbf{a}_j) / \beta)}$. Note that this corresponds to self-normalized importance sampling and does not require access to $Z(\mathbf{s})$.

4 Experiments

We evaluate our algorithm, CRR, on a number of challenging simulated manipulation and locomotion domains. Several of our tasks involve very high-dimensional action spaces as well as perception via

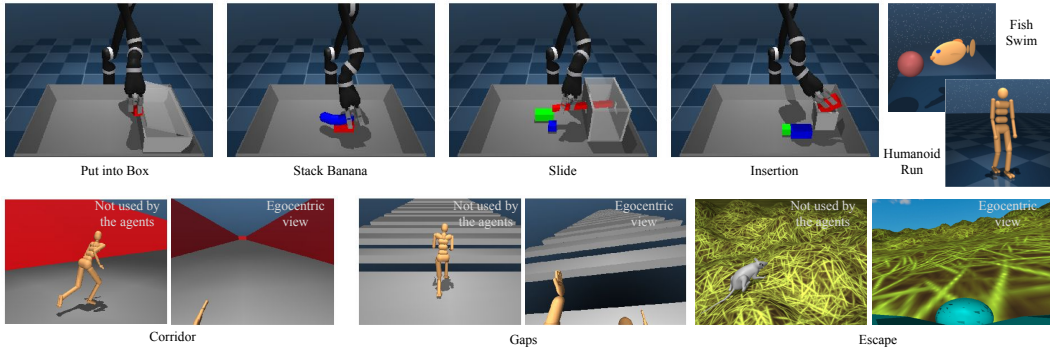


Figure 2: Illustrations of the environments. The agent has to solve the manipulation tasks using vision provided via 2 cameras. In the locomotion domains, a head-mounted egocentric camera is used to sense the surroundings. In the Deepmind control suite domains, no visual input is needed.

Table 2: Results on Deepmind Control suite. We divide the Deepmind control suite environments into two rough categories: easy (first 6) and hard (last 3).

	BC	D4PG	ABM	BCQ	CRR exp	CRR binary	CRR binary max
Cartpole Swingup	386 ± 6	855 ± 13	798 ± 30	444 ± 15	664 ± 22	860 ± 7	858 ± 15
Finger Turn Hard	261 ± 39	764 ± 24	566 ± 25	311 ± 38	714 ± 38	755 ± 31	833 ± 57
Walker Stand	386 ± 6	929 ± 46	689 ± 13	501 ± 5	797 ± 30	881 ± 13	929 ± 10
Walker Walk	417 ± 33	939 ± 19	846 ± 15	748 ± 24	901 ± 12	936 ± 3	951 ± 7
Cheetah Run	407 ± 56	308 ± 121	304 ± 32	368 ± 129	577 ± 79	453 ± 20	415 ± 26
Fish Swim	466 ± 8	281 ± 77	527 ± 19	473 ± 36	517 ± 21	585 ± 23	596 ± 11
Manipulator Insert Ball	385 ± 12	154 ± 54	409 ± 4	98 ± 29	625 ± 24	654 ± 42	636 ± 43
Manipulator Insert Peg	324 ± 31	71 ± 2	345 ± 12	194 ± 117	387 ± 36	365 ± 28	328 ± 24
Humanoid Run	382 ± 2	1 ± 1	302 ± 6	22 ± 3	586 ± 6	412 ± 10	226 ± 11

RGB cameras (subject to weak partial observability due to egocentricity in a locomoting body). Our results demonstrate that CRR works well even in these challenging settings and that it outperforms previously published approaches, in some cases by a considerable margin. We also perform several ablations that highlight the importance of individual algorithm components, and finally provide results on some toy domains that provide insight on why alternative approaches may fail.

4.1 Environments and datasets

We experiment with the continuous control tasks introduced in RL Unplugged (RLU) [3]. There are 17 different tasks in RLU: nine tasks from the Deepmind Control suite [34] and seven locomotion tasks. We additionally introduce four robotic manipulation datasets. The tasks cover a diverse set of scenarios, making our experimental study one of the most comprehensive to date for offline RL. All simulations are conducted using MuJoCo [35]; illustrations of the environments are given in Fig. 2.

Deepmind Control Suite (DCS). We consider the following tasks: *cartpole-swingup*, *walker-stand*, *walker-walk*, *cheetah-run*, *finger-turn-hard*, *manipulator-insert-ball*, *manipulator-insert-peg*, *fish-swim*, *humanoid-run*, all from the [DeepMind Control Suite](#). The data contains both successful and unsuccessful episodes. Many of these tasks are relatively straightforward with low action dimensions. Observations are given by features (no pixel observations nor partial observability). A number of these tasks are, however, quite challenging. Especially for the high-dimensional humanoid body, generating the dataset from several independent learning experiments lead to very diverse data: posing challenges for offline RL algorithms. For a split between easy and hard tasks, please see Table 2.

Locomotion. We further consider challenging [locomotion](#) tasks from RLU, for a humanoid [adapted from 13, 21] as well as for a rodent [adapted from 23]. The three humanoid tasks require running down the corridor at a target speed (*corridor* task), avoiding obstacles like walls (*walls* task) or gaps (*gaps* task). Data for these tasks is generated by training a hierarchical architecture that uses a pre-trained low-level controller (NPMP), following Merel et al. [22]. Note that we use the pre-trained controller only for generating the data sets but *not* in our offline experiments. For the rodent, there are four tasks comprising “escaping” from a hilly region (*escape* task), foraging in a maze (*forage* task), an interval timing task (*two-tap* task), and a size-proportionate version of the gaps task (*gaps* task) [for details, see 23]. As before, 3 independent online agent training runs are used to record the data for each of the tasks. The data is again of varying quality as it includes failed trajectories from early in training. This set of tasks is particularly challenging due to their high dimensional action spaces (56DoF for humanoid and 38DoF for the rodent). Additionally, the agent must observe the surroundings, to avoid obstacles, using an unstable egocentric camera (controlled via head and neck movements). Last but not least, a few tasks in this task suite are partially observable and thus require recurrent agents.

Robotic Manipulation. These tasks require the agent to control a simulated Kinova Jaco robotic arm (9DoF) to solve a number of manipulation problems. We use joint velocity control (at 20HZ) of all 6 arm joints and the 3 joints of the hand. The agent observes the proprioceptive features directly, but can only infer the objects on the table from pixel observations. Two camera views of size 64×64 are provided: one frontal camera covering the whole scene, and an in-hand camera for closeup of the objects. The episodes are of length 400 and the reward function is binary depending on whether the task is successfully executed. We consider 4 different challenges: *put into box*, *stack banana*,

Table 3: Results on Locomotion Suite. The first 3 tasks can be solved by feedforward agents; the corresponding datasets are not sequential. The last 4 tasks necessitate observation histories and all agents here are recurrent.

	BC	D4PG	ABM	CRR exp	CRR binary	CRR binary max
Humanoid Corridor	220 ± 194	4 ± 4	64 ± 3	918 ± 14	484 ± 97	245 ± 180
Humanoid Gaps	149 ± 9	5 ± 3	94 ± 9	546 ± 36	149 ± 89	33 ± 21
Rodent Gaps	463 ± 137	176 ± 6	420 ± 70	957 ± 19	492 ± 117	392 ± 6
Humanoid Walls	138 ± 77	2 ± 1	131 ± 25	422 ± 24	289 ± 72	232 ± 24
Rodent Escape	388 ± 3	24 ± 14	441 ± 16	428 ± 26	444 ± 45	499 ± 40
Rodent Mazes	343 ± 48	53 ± 1	478 ± 7	459 ± 7	464 ± 12	457 ± 13
Rodent Two Tap	325 ± 60	16 ± 2	598 ± 2	543 ± 32	615 ± 19	588 ± 14

slide and *insertion*. The dataset for each task is generated from 3 independent runs of a DPGfD agent (8000 episodes each).³

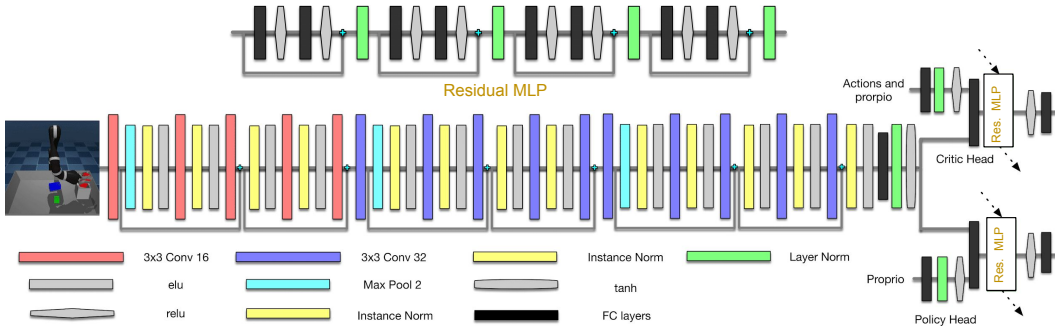


Figure 3: [TOP] Residual MLP used as a part of our network architecture. The black blocks indicated linear layers (of size 1024), green blocks layer-norm, and gray blocks ReLUs. [BOTTOM] Full CRR network. The residual MLP fits on top of the CRR networks. If recurrence is needed, we add two LSTM layers of size 1024 on top of the residual MLP layers before producing value and policy.

4.2 Experimental Setup

For environments where vision is involved we use ResNets to process the visual inputs. Proprioceptive information is concatenated with the output of the ResNets and the result is fed into a MLP with residual connections. The network structures are depicted in Fig. 3. The critic and policy networks share the vision modules and maintain separate copies of MLPs of identical structure, but employ different last layers to compute the Q and policy respectively. In our experiments, we use 4 residual blocks for the MLPs. For environments where vision is not required, we use the MLP alone. For CRR policies, we use a mixture of Gaussians policy head with 5 mixture components. Crucially, when evaluating CRR (and BC) policies, we turn off the noise in the Gaussian component distributions. We show this is essential in achieving good results in supplementary materials. We also provide additional details on our evaluation protocol in the appendix. For D4PG we compared using the same architecture as for CRR versus using the architecture from [14] and found the latter to be superior, so we used it for all experiments. The results are presented in Table 2, 3, and Figure 4.

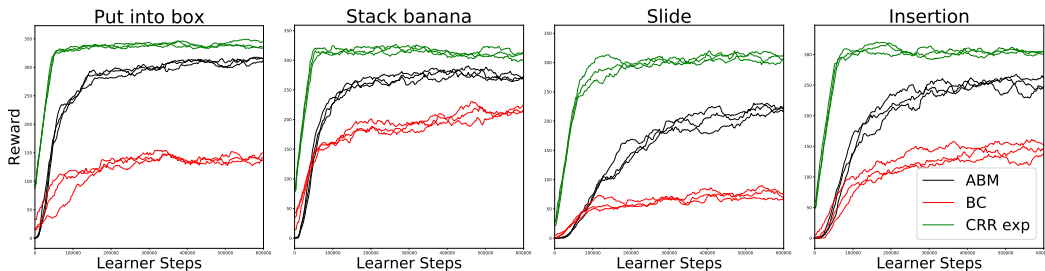


Figure 4: Results for CRR, ABM and BC on manipulation datasets. Only offline data is used during training.

³ Human demonstrations are used to train the DPGfD agents which additionally use distributional critics.

4.3 Analysis of CRR variants

In our experiments, we evaluate 3 variants of CRR which we call: *exp* (corresponding to Eqn. (4) with function f clipped to the maximal value of 20 for stability), *binary* (Eqn. (3)), and *binary max* (Eqn. (3)). The first two variants use \hat{A}_{mean} and the last one uses \hat{A}_{max} . Notice that all three variants do reasonably across all environments and their performance differ little in most environments.

When learning on low-complexity environments, however, CRR *binary* and especially CRR *binary max* are superior; see Table 2, row 1-4. We hypothesize that this is due to the fact that action filtering imposed by the *binary* (and more so for *binary max*) rule removes low-quality actions more aggressively. As the complexity of these environments is low, good policies can be learned from high quality data points, making CRR *binary* (max) particularly effective. In contrast, the *exp* rule tends to be too permissive and copies sub-optimal actions, leading to performance degradation.

Additionally, the relative value of an inferior action in the dataset compared to that of the policy tends to increase due to value overestimation. As training progresses, CRR therefore tends to copy more inferior actions as its policy improves. This could eventually lead to the decline of performance on some environments. In the appendix, we demonstrate the value overestimation phenomenon and introduce further analysis.

In contrast, for harder environments, where the task is difficult but high quality data is relatively abundant, CRR *exp* becomes superior. This may be explained by the fact that CRR *binary* filters out too many actions to adequately learn policies. For example, when training on the humanoid-run environment in DCS, CRR *binary* effectively considers, on average, 10%–12% of actions in the entire dataset and CRR *binary max* 2%–5%. We speculate that this explains the superior performance of CRR *exp* on the humanoid tasks in DCS and the locomotion suites. On all manipulation environments the *binary* indicator performs similar to the exponential version.

CWP generally improves the performance of CRR. Consequently, for all CRR variants we present only results with CWP and leave the ablation to the appendix.

4.4 Comparison to baselines

Comparison to D4PG. We compare CRR with a state-of-the-art off-policy RL algorithm for continuous control: D4PG [4]. D4PG has been used successfully to solve a variety of problems [34] as well as for learning from a combination of offline (and off-task) and online data [6]. It utilizes the same distributional critic as CRR, allowing us to isolate the effect of changing the policy losses. We tuned the network architectures of D4PG on a few control suite tasks and found that it favors smaller networks compared to those used for CRR. The two approaches otherwise differ only in the policy training and how bootstrapping is performed during policy evaluation (for D4PG we query $Q(s, a)$ at the policy mean while CRR employs a sample based approximation). Full details on the hyper-parameters are given in the appendix. The results on manipulation as well as the DCS domains are shown in Fig. 4 and Tables 2 and 3.

Overall, our results confirm previously published results that the naive application of off-policy RL algorithms can fail in the offline RL settings [9, 30]: **D4PG** performs well on some of the DCS domains, but fails on the domains with higher dimensional action spaces (*humanoid-run*, and problems on the locomotion suite). Here its performance is indistinguishable from a random policy. This is also consistent with the results of [2] who find that standard off-policy RL algorithms can perform well in the offline setting in some cases; presumably when the state-action space of the domain is well covered in the dataset.

Comparison to BCQ / ABM. We also compare to two recently published offline RL algorithms: BCQ [10] and ABM [30]. We used the hyperparameters listed in [10] for BCQ, including network architectures and hyperparameters. To better ablate the difference between CRR and ABM, we implemented ABM to use exactly the same architectures as CRR with the exception of using Gaussian policy heads for ABM to stay close to the original MPO formulation [1]. Our implementation of ABM is thus equipped with distributional critics and can use recurrent networks where appropriate. We adopt hyper-parameters specific to ABM from the original paper. (see supplementary for details).

Similar to D4PG, BCQ behaves reasonably well on the easier tasks on DCS. It, however, fails to make progress on harder tasks like *humanoid-run* and *manipulator-insert-ball*. For that reason we do not consider BCQ for more complicated environments.

ABM performs well on most control suite environments. Compared to CRR, however, it underperforms on the Humanoid Run task, as well as the humanoid tasks in the Locomotion Suite. These are the same tasks on which the performance of *CRR binary* is weaker, and we hypothesize that the lower performance can be explained by the structural similarity between *CRR bin* and the prior in *ABM* (see Section 3). Furthermore, the policy update in MPO is ineffective at reducing the stochasticity of the prior policy which can lower performance in humanoid and manipulation environments.

Comparison to Behavior Cloning. Although BC can work surprisingly well when high quality data for a task is available, its performance suffers in the presence of low-quality data. We use the same network architecture (without the critic network) and hyper-parameter as for CRR. This allows us to isolate the effect of the advantage-based filtering step that is part of CRR. As shown in the experiments, BC performs surprisingly well on a number of environments. Notably, unlike D4PG or BCQ, BC behaves reasonably well in environments with very high dimensional action spaces demonstrating its advantages over the RL losses. BC is, however, inferior to CRR or ABM overall.

5 Conclusion

We have presented an algorithm for offline RL that is simpler than existing methods but leads to surprisingly good performance even on challenging tasks. Our algorithm can be seen as a form of filtered behavioral cloning where data is selected based on information contained in the policy’s Q-function. We have investigated several variants of the algorithm. *CRR exp* performs especially well across the entire range of tasks considered. Our detailed evaluation has highlighted that design factors, such as the choice of filter, can have significant influence depending on the nature of the task. We have provided some preliminary explanations of these effects. Given the already promising performance of CRR we believe that studying the underlying dynamics further is a valuable direction for future work and has the potential to reveal further algorithmic improvements that may push the frontier of offline RL algorithms in terms of robustness, performance and simplicity.

Broader Impact

RL methods represent a unique solution principle that could lead to substantial progress in many real-world applications that are beneficial to society, such as the development of assistive robotic technologies for the disabled. As online RL and especially exploration is difficult (and sometimes dangerous) in the real world, offline RL provides a path for RL methods to be more broadly applied in practice. This paper introduces a new algorithm that could lead to improved performance on some real world tasks. As with all algorithms that can be used to automate decision making policies, however, offline RL methods could be used for applications with a negative impact on society. Since offline RL algorithms require existing datasets, we should also be vigilant when collecting datasets so as to avoid bias and prejudices.

References

- [1] Abbas Abdolmaleki, Jost Tobias Springenberg, Yuval Tassa, Remi Munos, Nicolas Heess, and Martin Riedmiller. Maximum a posteriori policy optimisation. In *International Conference on Learning Representations*, 2018.
- [2] Rishabh Agarwal, Dale Schuurmans, and Mohammad Norouzi. Striving for simplicity in off-policy deep reinforcement learning. *Preprint arXiv:1907.04543*, 2019.
- [3] Anonymous. RL unplugged: A suite of benchmarks for offline reinforcement learning. In *Submitted to NeurIPS 2020*, 2020.
- [4] Gabriel Barth-Maron, Matthew W. Hoffman, David Budden, Will Dabney, Dan Horgan, Dhruva TB, Alistair Muldal, Nicolas Heess, and Timothy Lillicrap. Distributional policy gradients. In *International Conference on Learning Representations*, 2018.
- [5] Marc G. Bellemare, Will Dabney, and Rémi Munos. A distributional perspective on reinforcement learning. In *International Conference on Machine Learning*, pages 449–458, 2017.

- [6] Serkan Cabi, Sergio Gómez Colmenarejo, Alexander Novikov, Ksenia Konyushkova, Scott Reed, Rae Jeong, Konrad Zolna, Yusuf Aytar, David Budden, Mel Vecerik, Oleg Sushkov, David Barker, Jonathan Scholz, Misha Denil, Nando de Freitas, and Ziyu Wang. Scaling data-driven robotics with reward sketching and batch reinforcement learning. *Preprint arXiv:1909.12200*, 2019.
- [7] Xinyue Chen, Zijian Zhou, Zheng Wang, Che Wang, Yanqiu Wu, Qing Deng, and Keith Ross. BAIL: Best-action imitation learning for batch deep reinforcement learning. *Preprint arXiv:1910.12179*, 2019.
- [8] Gabriel Dulac-Arnold, Daniel J. Mankowitz, and Todd Hester. Challenges of real-world reinforcement learning. *Preprint arXiv:1904.12901*, 2019.
- [9] Scott Fujimoto, Edoardo Conti, Mohammad Ghavamzadeh, and Joelle Pineau. Benchmarking batch deep reinforcement learning algorithms. *Preprint arXiv:1910.01708*, 2019.
- [10] Scott Fujimoto, David Meger, and Doina Precup. Off-policy deep reinforcement learning without exploration. In *International Conference on Machine Learning*, pages 2052–2062, 2019.
- [11] Yanjun Han, Jiantao Jiao, and Tsachy Weissman. Minimax estimation of discrete distributions. In *2015 IEEE International Symposium on Information Theory (ISIT)*, pages 2291–2295. IEEE, 2015.
- [12] Nicolas Heess, Gregory Wayne, David Silver, Tim Lillicrap, Tom Erez, and Yuval Tassa. Learning continuous control policies by stochastic value gradients. In *Conference on Neural Information Processing Systems*, pages 2944–2952, 2015.
- [13] Nicolas Heess, Dhruva Tirumala, Srinivasan Sriram, Jay Lemmon, Josh Merel, Greg Wayne, Yuval Tassa, Tom Erez, Ziyu Wang, S. M. Ali Eslami, Martin A. Riedmiller, and David Silver. Emergence of locomotion behaviours in rich environments. *Preprint arXiv:1707.02286*, 2017.
- [14] Matt Hoffman, Bobak Shahriari, John Aslanides, Gabriel Barth-Maron, Feryal Behbahani, Tamara Norman, Abbas Abdolmaleki, Albin Cassirer, Fan Yang, Kate Baumli, Sarah Henderson, Alex Novikov, Sergio Gómez Colmenarejo, Serkan Cabi, Caglar Gulcehre, Tom Le Paine, Andrew Cowie, Ziyu Wang, Bilal Piot, and Nando de Freitas. Acme: A research framework for distributed reinforcement learning. *Preprint arXiv:2006.00979*, 2020.
- [15] Natasha Jaques, Asma Ghandeharioun, Judy Hanwen Shen, Craig Ferguson, Àgata Lapedriza, Noah Jones, Shixiang Gu, and Rosalind W. Picard. Way off-policy batch deep reinforcement learning of implicit human preferences in dialog. *Preprint arXiv:1907.00456*, 2019.
- [16] Diederik P Kingma and Jimmy Ba. Adam: A method for stochastic optimization. *arXiv preprint arXiv:1412.6980*, 2014.
- [17] Aviral Kumar, Justin Fu, Matthew Soh, George Tucker, and Sergey Levine. Stabilizing off-policy Q-learning via bootstrapping error reduction. In *Conference on Neural Information Processing Systems*, pages 11761–11771, 2019.
- [18] Aviral Kumar, Xue Bin Peng, and Sergey Levine. Reward-conditioned policies. *Preprint arXiv:1912.13465*, 2019.
- [19] Sascha Lange, Thomas Gabel, and Martin Riedmiller. Batch reinforcement learning. In Marco Wiering and Martijn van Otterlo, editors, *Reinforcement Learning: State-of-the-Art*, pages 45–73. Springer Berlin Heidelberg, 2012.
- [20] Sergey Levine, Aviral Kumar, George Tucker, and Justin Fu. Offline reinforcement learning: Tutorial, review, and perspectives on open problems. *Preprint arXiv:2005.01643*, 2020.
- [21] Josh Merel, Arun Ahuja, Vu Pham, Saran Tunyasuvunakool, Siqi Liu, Dhruva Tirumala, Nicolas Heess, and Greg Wayne. Hierarchical visuomotor control of humanoids. In *International Conference on Learning Representations*, 2019.

- [22] Josh Merel, Leonard Hasenclever, Alexandre Galashov, Arun Ahuja, Vu Pham, Greg Wayne, Yee Whye Teh, and Nicolas Heess. Neural probabilistic motor primitives for humanoid control. In *International Conference on Learning Representations*, 2019.
- [23] Josh Merel, Diego Aldarondo, Jesse Marshall, Yuval Tassa, Greg Wayne, and Bence Ölveczky. Deep neuroethology of a virtual rodent. In *International Conference on Learning Representations*, 2020.
- [24] Volodymyr Mnih, Koray Kavukcuoglu, David Silver, Andrei A. Rusu, Joel Veness, Marc G. Bellemare, Alex Graves, Martin Riedmiller, Andreas K. Fidjeland, Georg Ostrovski, Stig Petersen, Charles Beattie, Amir Sadik, Ioannis Antonoglou, Helen King, Dharshan Kumaran, Daan Wierstra, Shane Legg, and Demis Hassabis. Human-level control through deep reinforcement learning. *Nature*, 518(7540):529–533, 2015.
- [25] Ashvin Nair, Bob McGrew, Marcin Andrychowicz, Wojciech Zaremba, and Pieter Abbeel. Overcoming exploration in reinforcement learning with demonstrations. *Preprint arXiv:1709.10089*, 2017.
- [26] Gerhard Neumann and Jan R. Peters. Fitted Q-iteration by advantage weighted regression. In *Conference on Neural Information Processing Systems*. 2009.
- [27] Xue Bin Peng, Aviral Kumar, Grace Zhang, and Sergey Levine. Advantage-weighted regression: Simple and scalable off-policy reinforcement learning. *Preprint arXiv:1910.00177*, 2019.
- [28] Dean A Pomerleau. ALVINN: An autonomous land vehicle in a neural network. In *Conference on Neural Information Processing Systems*, pages 305–313, 1989.
- [29] Stephane Ross, Geoffrey Gordon, and Drew Bagnell. A reduction of imitation learning and structured prediction to no-regret online learning. In *International Conference on Artificial Intelligence and Statistics*, 2011.
- [30] Noah Siegel, Jost Tobias Springenberg, Felix Berkenkamp, Abbas Abdolmaleki, Michael Neunert, Thomas Lampe, Roland Hafner, Nicolas Heess, and Martin Riedmiller. Keep doing what worked: Behavior modelling priors for offline reinforcement learning. In *International Conference on Learning Representations*, 2020.
- [31] David Silver, Guy Lever, Nicolas Heess, Thomas Degris, Daan Wierstra, and Martin A. Riedmiller. Deterministic policy gradient algorithms. In *International Conference on Machine Learning*, pages 387–395, 2014.
- [32] David Silver, Thomas Hubert, Julian Schrittwieser, Ioannis Antonoglou, Matthew Lai, Arthur Guez, Marc Lanctot, Laurent Sifre, Dharshan Kumaran, Thore Graepel, Timothy Lillicrap, Karen Simonyan, and Demis Hassabis. A general reinforcement learning algorithm that masters chess, shogi, and Go through self-play. *Science*, 362(6419):1140–1144, 2018.
- [33] Richard S. Sutton, David McAllester, Satinder Singh, and Yishay Mansour. Policy gradient methods for reinforcement learning with function approximation. In *Conference on Neural Information Processing Systems*, page 1057–1063, 1999.
- [34] Yuval Tassa, Yotam Doron, Alistair Muldal, Tom Erez, Yazhe Li, Diego de Las Casas, David Budden, Abbas Abdolmaleki, Josh Merel, Andrew Lefrancq, Timothy Lillicrap, and Martin Riedmiller. DeepMind control suite. *Preprint arXiv:1801.00690*, 2018.
- [35] Emanuel Todorov, Tom Erez, and Yuval Tassa. Mujoco: A physics engine for model-based control. In *International Conference on Intelligent Robots and Systems*, pages 5026–5033, 2012.
- [36] Hado van Hasselt and Marco Wiering. Reinforcement learning in continuous action spaces. In *ADPRL 2007*, 2020.
- [37] Qing Wang, Jiechao Xiong, Lei Han, peng sun, Han Liu, and Tong Zhang. Exponentially weighted imitation learning for batched historical data. In *Conference on Neural Information Processing Systems*, pages 6288–6297. 2018.

A Appendix

A.1 Analysis of CRR in the tabular setting

In this section, we show that in the tabular setting, CRR is safe and improves upon the behavior policy defined by the dataset. In addition, we show that as the dataset grows, the policies learned by CRR perform sensibly in the true underlying environment.

We assume that there is an underlying Markov Decision Process (MDP) $(\mathcal{S}, \mathcal{A}, P_{\mathcal{M}}, r, \gamma)$. For simplicity, We assume finite state and action spaces and a deterministic reward function $r : \mathcal{S} \times \mathcal{A} \rightarrow \mathbb{R}$.

Consider a dataset of the format $\mathcal{B} = \{(s_i, \mathbf{a}_i, s'_i)\}_i$. We assume the dataset is *coherent* (see [10]), meaning that if $(s_i, \mathbf{a}_i, s'_i) \in \mathcal{B}$, then $(s'_i, \mathbf{a}'_i, s''_i) \in \mathcal{B}$ for some \mathbf{a}'_i, s''_i unless s'_i is a terminal state.

Given the original MDP and data \mathcal{B} we define the associated *empirical MDP* $M_{\mathcal{B}}$ as in Section 4.1 of [10]: The empirical MDP shares the same action space (\mathcal{A}), and state space (\mathcal{S}) along with an additional terminal state s_{term} . $M_{\mathcal{B}}$ follows an empirical state transition probabilities:

$$P_{\mathcal{B}}(s'|s, \mathbf{a}) = \frac{N(s, \mathbf{a}, s')}{\sum_{\bar{s}} N(s, \mathbf{a}, \bar{s})}$$

where $N(s, \mathbf{a}, s')$ is the count of the appearance of s, \mathbf{a}, s' in the dataset. In the case where $\sum_{\bar{s}} N(s, \mathbf{a}, \bar{s}) = 0$, we set $P_{\mathcal{B}}(s_{term}|s, \mathbf{a}) = 1$ and set $r(s, \mathbf{a})$ to an arbitrary value. Assume that $(s, \mathbf{a}) \sim \mathcal{B}$, we define an empirical policy distribution

$$\mu_{\mathcal{B}}(\mathbf{a}|s) = \frac{N(\mathbf{a}, s)}{\sum_{\bar{\mathbf{a}}} N(\bar{\mathbf{a}}, s)},$$

where $N(\mathbf{a}, s) = \sum_{\bar{s}} N(\mathbf{a}, s, \bar{s})$. If $\sum_{\bar{\mathbf{a}}} N(\bar{\mathbf{a}}, s) = 0$, then let $\mu_{\mathcal{B}}(\cdot|s)$ be uniform. We also define $d_{\mathcal{B}}(s) = \frac{\sum_{\mathbf{a}, s'} N(s, \mathbf{a}, s')}{|\mathcal{B}|}$.

Given $M_{\mathcal{B}}$ and a policy π , we define the associated value functions

$$Q_{\mathcal{B}}^{\pi}(s, \mathbf{a}) = \mathbb{E}_{s_{t+i+1} \sim P_{\mathcal{B}}(\cdot|s_{t+i}, \mathbf{a}_{t+i}), \mathbf{a}_{t+i} \sim \pi(\cdot|s_{t+i})} \left[\sum_{i=0}^{\infty} \gamma^i r(s_{t+i}, \mathbf{a}_{t+i}) \mid s_t = s, \mathbf{a}_t = \mathbf{a} \right],$$

and $V_{\mathcal{B}}^{\pi}(s) = \mathbb{E}_{\mathbf{a} \sim \pi(\cdot|s)} Q_{\mathcal{B}}^{\pi}(s, \mathbf{a})$.

Given $Q_{\mathcal{B}}^{\pi_i}$, we consider the following CRR objectives in the tabular setting:

$$\begin{aligned} \text{Tab. CRR exp: } \pi_{i+1} &\leftarrow \arg \max_{\pi} \mathbb{E}_{s \sim d_{\mathcal{B}}} \left[\sum_{\mathbf{a}} Q_{\mathcal{B}}^{\pi_i}(s, \mathbf{a}) \pi(\mathbf{a}|s) \right] \\ &\text{subject to: } KL(\pi(\cdot|s) || \mu_{\mathcal{B}}(\cdot|s)) \leq \epsilon \quad \forall s \end{aligned} \quad (6)$$

$$\text{Tab. CRR binary: } \pi_{i+1} \leftarrow \arg \max_{\pi} \mathbb{E}_{s \sim d_{\mathcal{B}}} \left[\sum_{\mathbf{a}} \mathbb{1}_{[Q_{\mathcal{B}}^{\pi_i}(s, \mathbf{a}) \geq V^{\pi_i}(s)]} \mu_{\mathcal{B}}(\mathbf{a}|s) \log \pi(\mathbf{a}|s) \right]. \quad (7)$$

Notice that the Tabular CRR exp objective looks different from the learning rule defined by Eqn. 4. However, it is easy to show that (using the KKT conditions)

$$\pi_{i+1}(\mathbf{a}|s) = \frac{\exp\left(\frac{Q_{\mathcal{B}}^{\pi_i}(s, \mathbf{a}) - V^{\pi_i}(s)}{\beta(s)}\right) \mu_{\mathcal{B}}(\mathbf{a}|s)}{Z^{\pi_{i+1}}(s)}, \quad (8)$$

where $\beta(s)$ is a state dependent factor and $Z^{\pi_{i+1}}(s)$ the normalization constant. This equation is in a much more familiar form albeit with a state dependent $\beta(s)$.

With the tabular CRR objectives defined, we introduce the CRR algorithms in the tabular setting as presented in Algorithm 2.

To illustrate why CRR is safe in the offline setting, we first show that policies trained via CRR (in the $M_{\mathcal{B}}$) would not try actions not present in the dataset.

Algorithm 2: Tabular Critic Regularized Regression

Input: Empirical MDP $M_{\mathcal{B}}$, and empirical policy $\mu_{\mathcal{B}}$

Start with $\pi_0 = \mu_{\mathcal{B}}$

for $i \in \{1, \dots, \infty\}$ **do**

 Evaluate $Q_{\mathcal{B}}^{\pi_i}$ in the empirical MDP

 Compute π_{i+1} according to Equation (6) or (7)

end

Proposition 1. $\text{supp } \pi_i(\cdot|\mathbf{s}) \subseteq \text{supp } \mu_{\mathcal{B}}(\cdot|\mathbf{s}) \quad \forall i \geq 1, \mathbf{s} \in \mathcal{B}$ for Tabular CRR exp (binary) objectives.

Proof. We show the correctness of the statement only for the tabular CRR exp objective to avoid redundancy. Following Eqn. 8, we see that whenever $\mu_{\mathcal{B}}(\mathbf{a}|\mathbf{s}) = 0$, we have $\pi_{i+1}(\mathbf{a}|\mathbf{s}) = 0$. \square

In addition to being safe, we show that each iteration of CRR improves performance.

Proposition 2. (Policy improvement) When using the Tabular CRR binary objective, $Q_{\mathcal{B}}^{\pi_{i+1}}(\mathbf{s}, \mathbf{a}) \geq Q_{\mathcal{B}}^{\pi_i}(\mathbf{s}, \mathbf{a}) \quad \forall \mathbf{s}, \mathbf{a}$.

Proof. Define

$$q_{i+1}(\mathbf{a}|\mathbf{s}) = \frac{\mathbb{1}_{[Q_{\mathcal{B}}^{\pi_i}(\mathbf{s}, \mathbf{a}) \geq V^{\pi_i}(\mathbf{s})]} \mu_{\mathcal{B}}(\mathbf{a}|\mathbf{s})}{Z^{\pi_{i+1}}(\mathbf{s})}$$

where $Z^{\pi_{i+1}}(\mathbf{s})$ is the partition function. Then it is easy to see that

$$\begin{aligned} & \arg \max_{\pi} \mathbb{E}_{\mathbf{s} \sim d_{\mathcal{B}}} \left[\sum_{\mathbf{a}} \mathbb{1}_{[Q_{\mathcal{B}}^{\pi_i}(\mathbf{s}, \mathbf{a}) \geq V^{\pi_i}(\mathbf{s})]} \mu_{\mathcal{B}}(\mathbf{a}|\mathbf{s}) \log \pi(\mathbf{a}|\mathbf{s}) \right] \\ &= \arg \max_{\pi} \mathbb{E}_{\mathbf{s} \sim d_{\mathcal{B}}} \left[KL(q_{i+1}(\cdot|\mathbf{s}) || \pi(\cdot|\mathbf{s})) \right]. \end{aligned}$$

Therefore we have

$$\pi_{i+1}(\mathbf{a}|\mathbf{s}) = \frac{\mathbb{1}_{[Q_{\mathcal{B}}^{\pi_i}(\mathbf{s}, \mathbf{a}) \geq V^{\pi_i}(\mathbf{s})]} \mu_{\mathcal{B}}(\mathbf{a}|\mathbf{s})}{Z^{\pi_{i+1}}(\mathbf{s})}.$$

From the above equation, it is easy to see that $\forall \mathbf{a} \in \text{supp } \pi_{i+1}(\cdot|\mathbf{s}), Q_{\mathcal{B}}^{\pi_i}(\mathbf{s}, \mathbf{a}) \geq V^{\pi_i}(\mathbf{s})$. Therefore $\sum_{\mathbf{a}} \pi_{i+1}(\mathbf{a}|\mathbf{s}) Q_{\mathcal{B}}^{\pi_i}(\mathbf{s}, \mathbf{a}) \geq V^{\pi_i}(\mathbf{s}) = \sum_{\mathbf{a}} \pi_i(\mathbf{a}|\mathbf{s}) Q_{\mathcal{B}}^{\pi_i}(\mathbf{s}, \mathbf{a})$.

$$\begin{aligned} & Q_{\mathcal{B}}^{\pi_i}(\mathbf{s}, \mathbf{a}) \\ &= \mathbb{E} \left[r(\mathbf{s}_t, \mathbf{a}_t) + \gamma \sum \pi_i(\mathbf{a}_{t+1}|\mathbf{s}_{t+1}) Q_{\mathcal{B}}^{\pi_i}(\mathbf{s}_t, \mathbf{a}_t) \middle| \mathbf{s}_t = \mathbf{s}, \mathbf{a}_t = \mathbf{a} \right] \\ &\leq \mathbb{E} \left[r(\mathbf{s}_t, \mathbf{a}_t) + \gamma \sum \pi_{i+1}(\mathbf{a}_{t+1}|\mathbf{s}_{t+1}) Q_{\mathcal{B}}^{\pi_i}(\mathbf{s}_t, \mathbf{a}_t) \middle| \mathbf{s}_t = \mathbf{s}, \mathbf{a}_t = \mathbf{a} \right] \\ &\quad \dots \\ &\leq \mathbb{E}_{\pi_{i+1}} \left[\sum_{k=0}^{\infty} \gamma^k r(\mathbf{s}_{t+k}, \mathbf{a}_{t+k}) \middle| \mathbf{s}_t = \mathbf{s}, \mathbf{a}_t = \mathbf{a} \right] \\ &= Q_{\mathcal{B}}^{\pi_{i+1}}(\mathbf{s}, \mathbf{a}). \end{aligned}$$

\square

Proposition 3. (Policy improvement) When using the Tabular CRR exp objective, $Q_{\mathcal{B}}^{\pi_{i+1}}(\mathbf{s}, \mathbf{a}) \geq Q_{\mathcal{B}}^{\pi_i}(\mathbf{s}, \mathbf{a}) \quad \forall \mathbf{s}, \mathbf{a}$.

Proof. We have that $KL(\pi_i(\cdot|\mathbf{s})||\mu_{\mathcal{B}}(\cdot|\mathbf{s})) \leq \epsilon \forall \mathbf{s}$. Since

$$\pi^{i+1} = \arg \max_{\pi} \mathbb{E}_{\mathbf{s} \sim d_{\mathcal{B}}} \left[\sum_{\mathbf{a}} Q_{\mathcal{B}}^{\pi_i}(\mathbf{s}, \mathbf{a}) \pi(\mathbf{a}|\mathbf{s}) \right] \text{ s.t. } KL(\pi(\cdot|\mathbf{s})||\mu_{\mathcal{B}}(\cdot|\mathbf{s})) \leq \epsilon \forall \mathbf{s},$$

we know that $\sum_{\mathbf{a}} Q_{\mathcal{B}}^{\pi_i}(\mathbf{s}, \mathbf{a}) \pi_{i+1}(\mathbf{a}|\mathbf{s}) \geq \sum_{\mathbf{a}} Q_{\mathcal{B}}^{\pi_i}(\mathbf{s}, \mathbf{a}) \pi_i(\mathbf{a}|\mathbf{s}) \forall \mathbf{s}$.

It is easy to show that

$$\begin{aligned} & Q_{\mathcal{B}}^{\pi_i}(\mathbf{s}, \mathbf{a}) \\ &= \mathbb{E} \left[r(\mathbf{s}_t, \mathbf{a}_t) + \gamma \sum \pi_i(\mathbf{a}_{t+1}|\mathbf{s}_{t+1}) Q_{\mathcal{B}}^{\pi_i}(\mathbf{s}_t, \mathbf{a}_t) \middle| \mathbf{s}_t = \mathbf{s}, \mathbf{a}_t = \mathbf{a} \right] \\ &\leq \mathbb{E} \left[r(\mathbf{s}_t, \mathbf{a}_t) + \gamma \sum \pi_{i+1}(\mathbf{a}_{t+1}|\mathbf{s}_{t+1}) Q_{\mathcal{B}}^{\pi_i}(\mathbf{s}_t, \mathbf{a}_t) \middle| \mathbf{s}_t = \mathbf{s}, \mathbf{a}_t = \mathbf{a} \right] \\ &\quad \dots \\ &\leq \mathbb{E}_{\pi_{i+1}} \left[\sum_{k=0}^{\infty} \gamma^k r(\mathbf{s}_{t+k}, \mathbf{a}_{t+k}) \middle| \mathbf{s}_t = \mathbf{s}, \mathbf{a}_t = \mathbf{a} \right] \\ &= Q_{\mathcal{B}}^{\pi_{i+1}}(\mathbf{s}, \mathbf{a}). \end{aligned}$$

□

Finally we show that the difference in Q values for a given policy π between the ground truth MDP and the empirical MDP reduces as $|\mathcal{B}|$ increases. This allows us to conclude that the policies learned in the empirical MDP $M_{\mathcal{B}}$ is also a sensible policy in the original MDP.

Proposition 4. *Consider*

$$\epsilon_{MDP}(\mathbf{s}, \mathbf{a}) = Q^{\pi}(\mathbf{s}, \mathbf{a}) - Q_{\mathcal{B}}^{\pi}(\mathbf{s}, \mathbf{a}).$$

Define sets defined as $S(\mathbf{s}, \mathbf{a}) = \{(\bar{\mathbf{s}}, \bar{\mathbf{a}}, \bar{\mathbf{s}}') \in \mathcal{B} \mid \bar{\mathbf{s}} = \mathbf{s}, \bar{\mathbf{a}} = \mathbf{a}\}$. If as $|\mathcal{B}| \rightarrow \infty$, $S(\mathbf{s}, \mathbf{a}) = \emptyset$ or $|S(\mathbf{s}, \mathbf{a})| \rightarrow \infty$, and $\bar{\mathbf{s}}'$ is an i.i.d sample of $P(\cdot|\bar{\mathbf{a}}, \bar{\mathbf{s}}) \forall (\bar{\mathbf{s}}, \bar{\mathbf{a}}, \bar{\mathbf{s}}') \in \mathcal{B}$, then

$$\text{as } |\mathcal{B}| \rightarrow \infty, \sup_{\substack{\mathbf{s} \in \text{supp } d_{\mathcal{B}} \\ \mathbf{a} \in \text{supp } \pi(\cdot|\mathbf{s})}} \epsilon_{MDP}(\mathbf{s}, \mathbf{a}) \rightarrow 0.$$

Proof. From Lemma 1 in [10], we have

$$\begin{aligned} & \epsilon_{MDP}(\mathbf{s}, \mathbf{a}) \\ &= \sum_{\mathbf{s}'} (P_{\mathcal{M}}(\mathbf{s}'|\mathbf{s}, \mathbf{a}) - P_{\mathcal{B}}(\mathbf{s}'|\mathbf{s}, \mathbf{a})) \left(r + \gamma V_{\mathcal{B}}^{\pi}(\mathbf{s}') \right) + \\ & \quad \gamma \sum_{\mathbf{s}'} (P_{\mathcal{M}}(\mathbf{s}'|\mathbf{s}, \mathbf{a}) - P_{\mathcal{B}}(\mathbf{s}'|\mathbf{s}, \mathbf{a})) \sum_{\mathbf{a}'} \pi(\mathbf{a}'|\mathbf{s}') \epsilon_{MDP}(\mathbf{s}', \mathbf{a}') + \\ & \quad \gamma \sum_{\mathbf{s}'} P_{\mathcal{B}}(\mathbf{s}'|\mathbf{s}, \mathbf{a}) \sum_{\mathbf{a}'} \pi(\mathbf{a}'|\mathbf{s}') \epsilon_{MDP}(\mathbf{s}', \mathbf{a}') \end{aligned}$$

Since \mathcal{B} is coherent, we have

$$\begin{aligned} & \epsilon_{MDP}(\mathbf{s}, \mathbf{a}) \\ &\leq \sum_{\mathbf{s}'} (P_{\mathcal{M}}(\mathbf{s}'|\mathbf{s}, \mathbf{a}) - P_{\mathcal{B}}(\mathbf{s}'|\mathbf{s}, \mathbf{a})) \left(r + \gamma V^{\pi}(\mathbf{s}') \right) + \\ & \quad \gamma \sup_{\substack{\mathbf{s} \in \text{supp } d_{\mathcal{B}} \\ \mathbf{a} \in \text{supp } \pi(\cdot|\mathbf{s})}} \epsilon_{MDP}(\mathbf{s}, \mathbf{a}) \end{aligned}$$

for all $\mathbf{s} \in \text{supp } d_{\mathcal{B}}, \mathbf{a} \in \text{supp } \pi(\cdot|\mathbf{s})$. Taking the supremum on both sides:

$$\begin{aligned} & \sup_{\substack{\mathbf{s} \in \text{supp } d_{\mathcal{B}} \\ \mathbf{a} \in \text{supp } \pi(\cdot|\mathbf{s})}} \epsilon_{MDP}(\mathbf{s}, \mathbf{a}) \\ &\leq \sup_{\substack{\mathbf{s} \in \text{supp } d_{\mathcal{B}} \\ \mathbf{a} \in \text{supp } \pi(\cdot|\mathbf{s})}} \sum_{\mathbf{s}'} (P_{\mathcal{M}}(\mathbf{s}'|\mathbf{s}, \mathbf{a}) - P_{\mathcal{B}}(\mathbf{s}'|\mathbf{s}, \mathbf{a})) \left(r + \gamma V^{\pi}(\mathbf{s}') \right) \\ & \quad + \gamma \sup_{\substack{\mathbf{s} \in \text{supp } d_{\mathcal{B}} \\ \mathbf{a} \in \text{supp } \pi(\cdot|\mathbf{s})}} \epsilon_{MDP}(\mathbf{s}', \mathbf{a}'). \end{aligned}$$

Rearranging the terms:

$$\begin{aligned} & \sup_{\substack{\mathbf{s} \in \text{supp } d_{\mathcal{B}} \\ \mathbf{a} \in \text{supp } \pi(\cdot|\mathbf{s})}} \epsilon_{MDP}(\mathbf{s}, \mathbf{a}) \\ & \leq \sup_{\substack{\mathbf{s} \in \text{supp } d_{\mathcal{B}} \\ \mathbf{a} \in \text{supp } \pi(\cdot|\mathbf{s})}} \frac{1}{1-\gamma} \sum_{\mathbf{s}'} (P_{\mathcal{M}}(\mathbf{s}'|\mathbf{s}, \mathbf{a}) - P_{\mathcal{B}}(\mathbf{s}'|\mathbf{s}, \mathbf{a})) \left(r + \gamma V^{\pi}(\mathbf{s}') \right). \end{aligned}$$

Let $R_{\max} = \frac{1}{1-\gamma} \max_{\mathbf{s}, \mathbf{a}} |r(\mathbf{s}, \mathbf{a})|$, we then have by Hölder’s inequality

$$\sup_{\substack{\mathbf{s} \in \text{supp } d_{\mathcal{B}} \\ \mathbf{a} \in \text{supp } \pi(\cdot|\mathbf{s})}} \epsilon_{MDP}(\mathbf{s}, \mathbf{a}) \leq \sup_{\substack{\mathbf{s} \in \text{supp } d_{\mathcal{B}} \\ \mathbf{a} \in \text{supp } \pi(\cdot|\mathbf{s})}} \frac{R_{\max}}{1-\gamma} \sum_{\mathbf{s}'} |P_{\mathcal{M}}(\mathbf{s}'|\mathbf{s}, \mathbf{a}) - P_{\mathcal{B}}(\mathbf{s}'|\mathbf{s}, \mathbf{a})|.$$

since $|S(\mathbf{s}, \mathbf{a})| \rightarrow \infty$ as $|\mathcal{B}| \rightarrow \infty$ for all $\mathbf{s} \in \text{supp } d_{\mathcal{B}}$ $\mathbf{a} \in \text{supp } \pi(\cdot|\mathbf{s})$, we have $\sup_{\substack{\mathbf{s} \in \text{supp } d_{\mathcal{B}} \\ \mathbf{a} \in \text{supp } \pi(\cdot|\mathbf{s})}} \sum_{\mathbf{s}'} |P_{\mathcal{M}}(\mathbf{s}'|\mathbf{s}, \mathbf{a}) - P_{\mathcal{B}}(\mathbf{s}'|\mathbf{s}, \mathbf{a})| \rightarrow 0$ by Theorem 1 of [11]. \square

A.2 Evaluation protocol

To compute the performance of each agent, as reported in the Tables 2, 3,5, 6 and 7, we adopt the following procedure. We run each agent with three independent seeds. Agent snapshots are made every 50000 learner steps. For every agent / environment / seed combination, we evaluate all its saved snapshots by running each for 300 episodes in the environment and record the mean episodic reward of the best snapshot as an agent’s performance for the seed. The performance of an agent in an environment is thus calculated as the mean performance across its seeds, and error bars the standard deviation of the means.

A.3 Effects of using K-step returns

In this section, we evaluate the effect of using K-step returns compared to our proposed method of estimating advantages. As discussed in Sec. 3 using K-step returns can hurt the agent’s performance since the transitions stored in the dataset are likely to be generated by very different policies than the current one. As a result, K-step returns may not reflect the actual returns of the current policy being evaluated and therefore introduce a bias. To test this hypothesis, we evaluate CRR’s (using the *binary max* rule) performance while estimating the advantage by

$$\sum_{i=0}^{k-1} \gamma^i r_{t+i} + \gamma^k \frac{1}{m} \sum_{j=1}^m Q_{\theta}(\mathbf{s}_{t+k}, \tilde{\mathbf{a}}_{t+k}^j) - \frac{1}{m} \sum_{j=1}^m Q_{\theta}(\mathbf{s}_t, \tilde{\mathbf{a}}_t^j)$$

where $\tilde{\mathbf{a}}_{t+k}^j \sim \pi(\mathbf{s}_{t+k})$, and $\tilde{\mathbf{a}}_t^j \sim \pi(\mathbf{s}_t)$. This objective is similar to the ones used in [27, 7].

As shown in Fig. 5, when choosing $k = 5$, we indeed observe an degradation in performance. This confirms that, with a large enough k , K-step returns produce a bias that compromises learning.

A.4 Hyper-parameters

In this section, we describe the hyper-parameters of algorithms used.

A.4.1 BCQ

For BCQ, we mostly follow the original network architecture as well as hyper-parameter settings in our implementation. Please refer to [10] for more details. We only changed the batch size to be 1024 to stay compatible with CRR.

A.4.2 CRR

For CRR training we use: target network update period 100; 21 atoms on a grid from 0 to 100 for the distributional critic. We use $\beta = 1$ for Eqn. (4) and for CWP resampling. We swept β

over $[0.1, 0.4, 0.7, 1, 1, 3]$ on few selected environments and did not find it to affect the results too much and therefore kept the natural setting of $\beta = 1$. For all experiments, we use 2 separate Adam optimizers [16] for actor and critic learning respectively. The learning rates are set to 10^{-4} . For sequence datasets, we use the batch size of 128 and for non-sequence datasets 1024. To compute the advantage estimates (see Table 1), we set $m = 4$.

For the descriptions of the network architecture, please see Figure 3. On the manipulation suite, two camera observations are provided in each time step. In these environments, we duplicate the entire lower stack of the network before the concatenation with proprioceptive (action) features to accommodate the extra pixel observation.

A.4.3 D4PG

For both the actor and critic, we use the Adam optimizer [16] with the learning rate of $1e-4$; target network update period 100; 51 atoms on a grid from -150 to 150 for the distributional critic. We use D4PG implemented in Acme [14], following their network architectures and hyper-parameters. We used batch size 1024 for experiments on the manipulation suite and 256 for the rest of experiments. We experimented with CRR’s network and hyper-paramters for D4PG, but the performance is inferior.

A.4.4 BC

Our BC implementation shares of its hyper-parameters with CRR whenever applicable. Most hyper-parameters, however, do not apply to BC. Our BC implementation shares the same policy network structure with CRR.

A.4.5 ABM

For ABM training we use mostly the same hyperparameters as CRR. ABM uses an additional prior policy network to train which we also use an Adam optimizer with learning rate 10^{-4} . To compute the advantage estimates for ABM, we set use 20 samples as per the original paper. For ABM specific hyper-parameters, the please see Table 4.

Our ABM implementation shares the same network architecture with CRR with the exception of its policy head being Gaussian. For the descriptions of the network architecture, please see Figure 3.

A.5 Value over-estimation

In section 4.3, we mention that the relative value of actions in the dataset compared to that of the policy tends to increase due to value overestimation (for actions present in the dataset). We hypothesize that this is due to the following effect. As the CRR policy gets better, the value of the

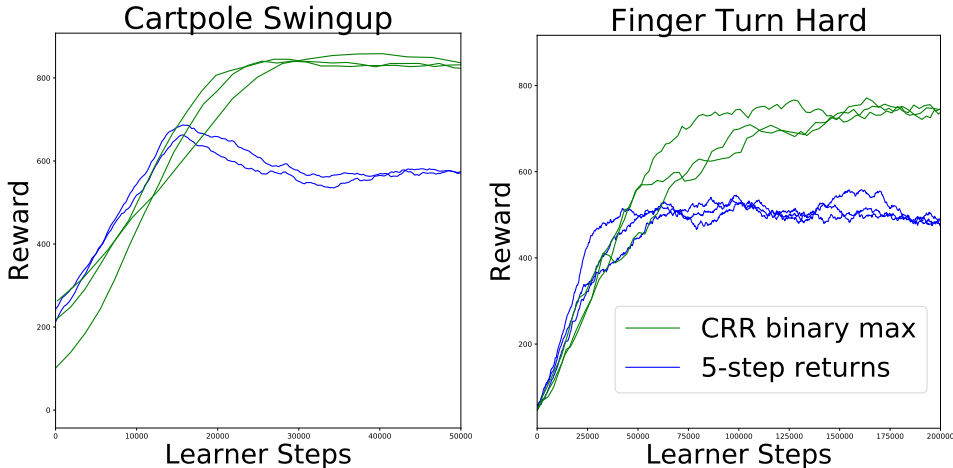


Figure 5: Evaluating the effect of K -step returns ($K = 5$ in this case). In offline RL, K -step returns could be detrimental as it introduces a bias. Here we see that using K -step returns hurts policy performance.

Table 4: ABM specific hyper-parameters.

Hyper-parameters	values
Number of actions sampled per state	20
ϵ	0.1
ϵ_μ	5×10^{-3}
ϵ_Σ	1×10^{-5}

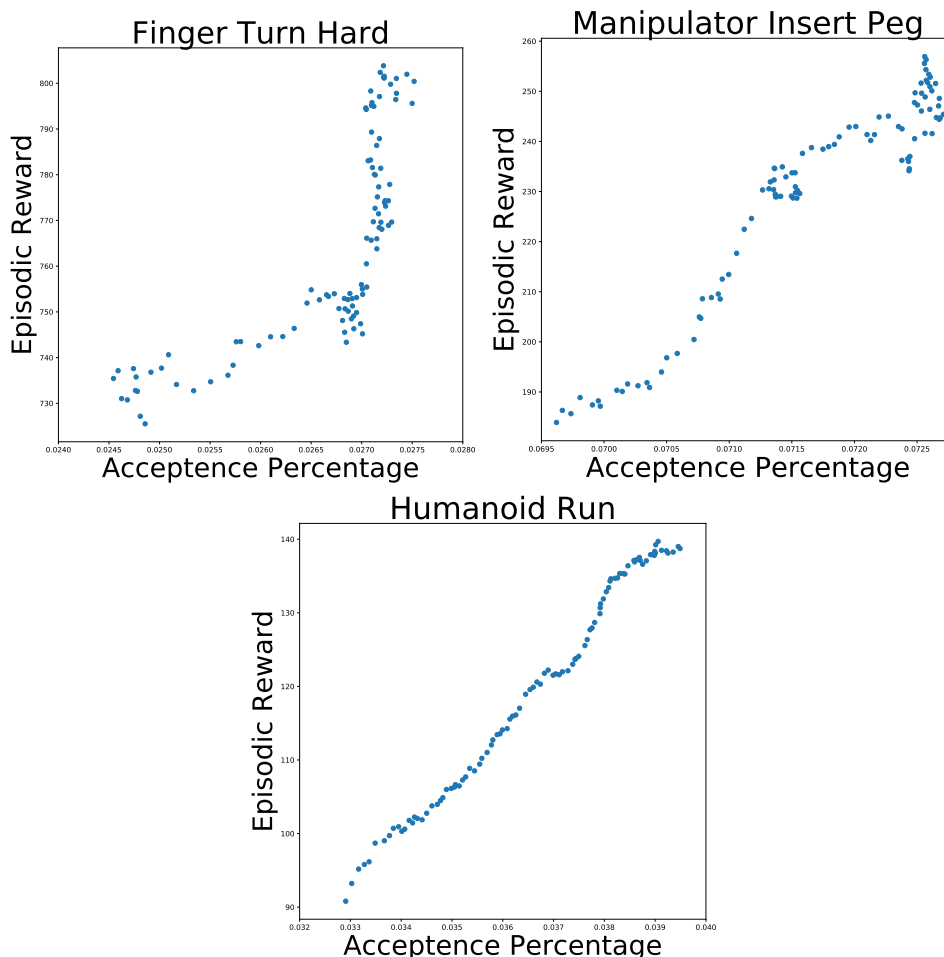


Figure 6: Here we compare the percentage of accepted actions under the *binary max* rule versus agents’ performance measured by episodic return. Surprisingly, the two quantities are positively correlated suggesting that the values of some actions in the dataset are overestimated compared to that of the policy.

bootstrap target (in critic learning) increases. As a result, the Q values for actions in the dataset, even that of suboptimal actions, also increase. As a result some of the suboptimal actions would have values higher than the value of the current policy.

We demonstrate this effect by comparing the percentage of actions copied using the *binary max* rule versus the agents’ performance measured in terms of episodic return. In these experiments, we evaluate the agents’ performance between 200000 and 600000 learner steps. We do not include datapoints corresponding to fewer than 2000000 learner steps in this analysis since early in learning the critic may not be reliable. We, in addition, measure how the percentage of actions copied by the *binary max* rule in the same learner steps range.

Intuitively, as the agent’s performance improves, we would expect the dataset to contain fewer actions that outperform the agent’s policy. Thus, the fraction of actions included in the policy update in

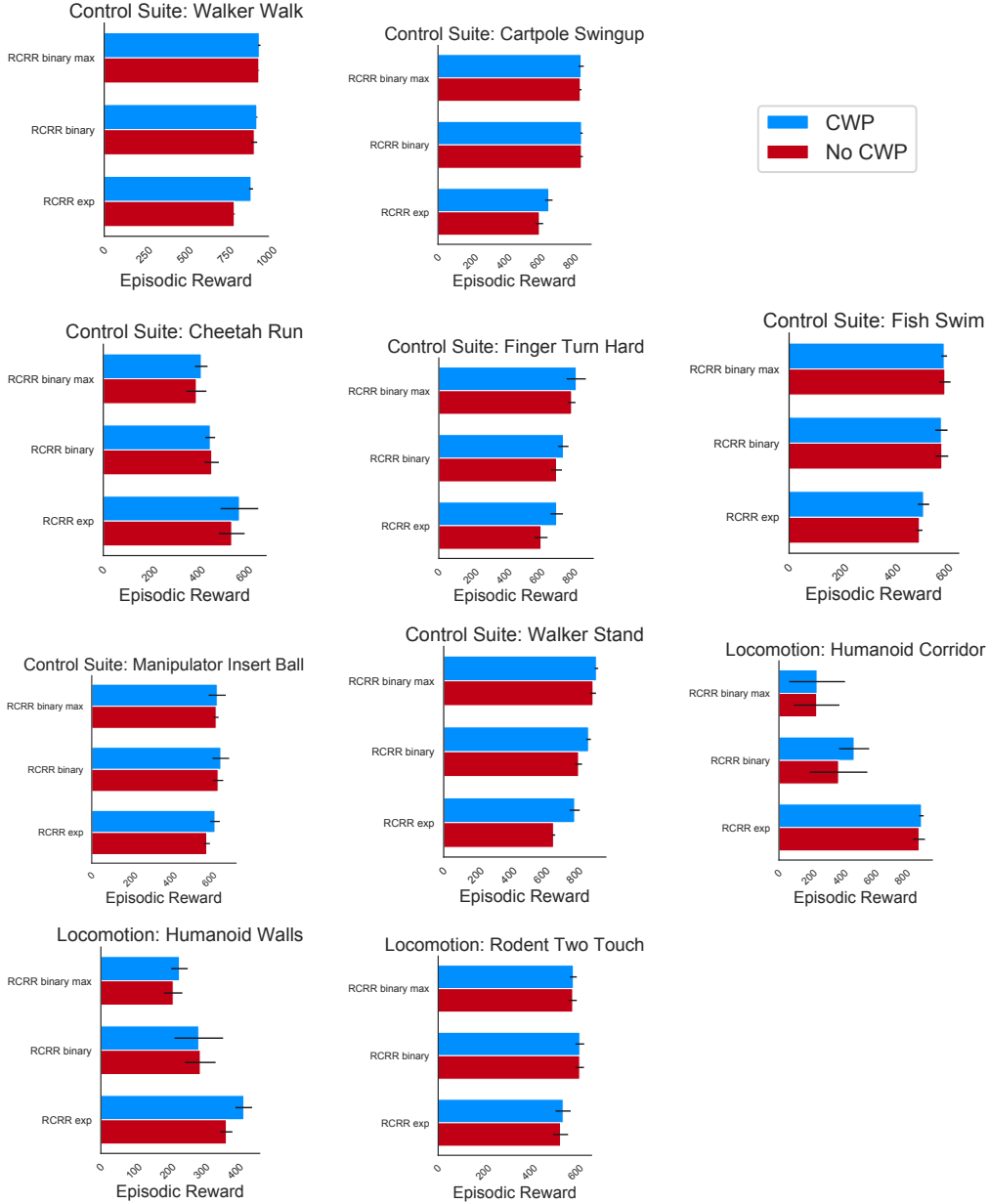


Figure 7: CWP ablation on selected environments. In these environments, we find CWP to mostly help and when it does not, CWP also do not hurt policy performance.

Eqn. 3 should go down. We do observe the opposite (as shown in Figure 6), however: the number of actions that are included in the policy update *increases* as agent performance improves. This supports our theory that the value of some actions from the datasets are overestimated compared to the value of the policy.

Due to the relative overestimation of the datasets' actions' values, CRR could clone sub-optimal actions leading to degradation in performance. The *binary max* rule, by being optimistic about the policy's state-value, copies fewer sub-optimal actions and thereby increases CRR's performance on some datasets.

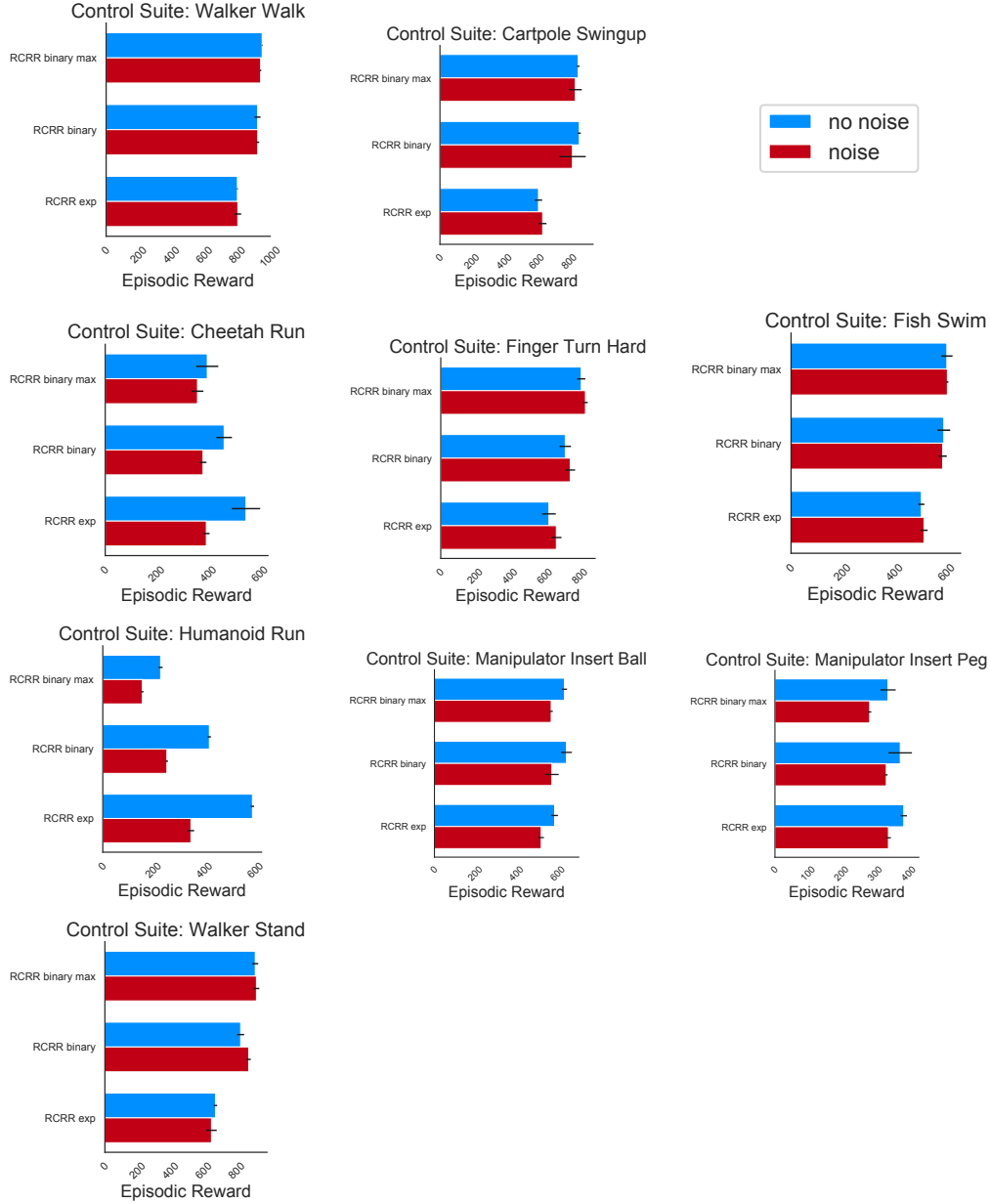


Figure 8: Control suite policy noise ablation.

A.6 Effect of noise when running the policy.

As mentioned in Section 4.2, we turn off the noise of component Gaussian distributions when evaluating policies. In Figure 8 and 9, we compare the effect of turning off the noise versus not. When it comes to environments of low and moderate action dimensionality, having no noise is beneficial, but often its effect is not significant. For examples, see results for *cartpole swingup*, *walker stand*, *cheetah run* in Figure 8.

For some environments the effect of noise is pronounced. This is clearly visible in Fig. 9 for instance. For the humanoid environments in the locomotion suite, the task is terminated when the humanoid falls. This makes it hard to recover from mistakes and may put policies with a high-level of stochasticity at a disadvantage. Overall, turning off the noise rarely adversely affect the agents' performance.

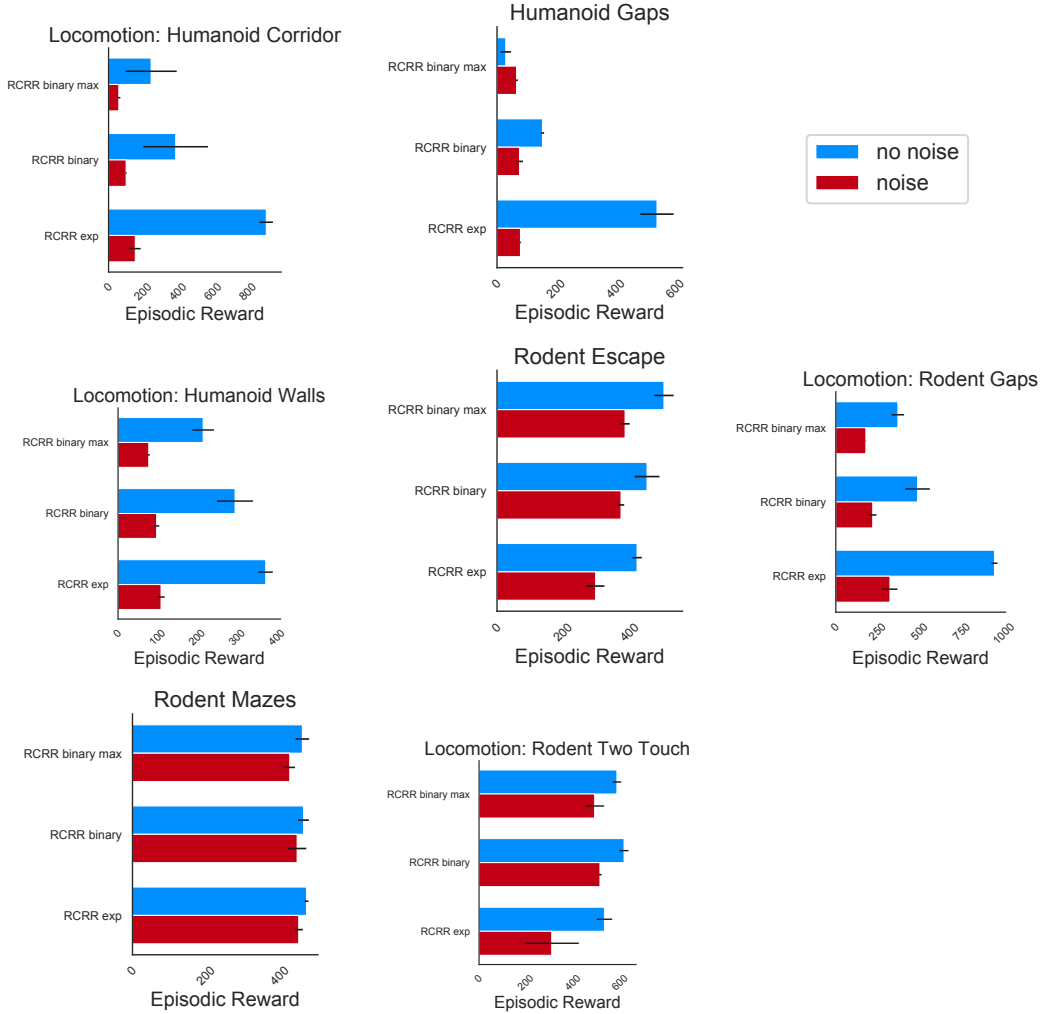


Figure 9: Locomotion policy noise ablation.

A.7 CWP Ablation

In this section we ablate the effect of CWP. Notice, when using CWP, we also turn off the component Gaussian distributions’ noise as described in the previous section. As we use mixture of Gaussians policies, CWP essentially chooses between the mean actions of the component Gaussians.

For the full list of results, please refer to Tables 5, 6, and 7. In Figure 7, we pick a few representative environments to illustrate CWP’s effect. As shown in the results, CWP generally helps with its effect especially pronounced when the policies’ performance is less than ideal. When CWP does not help, it also does not lower policy performance. CWP, however, does require more computation. We therefore recommend CWP whenever it is not too expensive to execute.

A.8 Full results table

Finally, we present all agents’ performance in Tables 5, 6, and 7.

Table 5: Results on Deepmind Control suite. We divide the Deepmind control suite environments into two rough categories: easy (first 6) and hard (last 3).

	BC	D4PG	RABM	BCQ	RCRR exp no-CWP	RCRR exp	RCRR binary no-CWP	RCRR binary	RCRR binary max no-CWP	RCRR binary max
Cartpole Swingup	386 ± 6	855 ± 13	798 ± 30	444 ± 15	607 ± 22	664 ± 22	859 ± 9	860 ± 7	853 ± 7	858 ± 15
Finger Turn Hard	261 ± 39	764 ± 24	566 ± 25	311 ± 38	620 ± 39	714 ± 38	714 ± 32	755 ± 31	805 ± 23	833 ± 57
Walker Stand	386 ± 6	929 ± 46	689 ± 13	501 ± 5	668 ± 10	797 ± 30	820 ± 21	881 ± 13	908 ± 17	929 ± 10
Walker Walk	417 ± 33	939 ± 19	846 ± 15	748 ± 24	798 ± 2	901 ± 12	920 ± 18	936 ± 3	949 ± 1	951 ± 7
Cheetah Run	407 ± 56	308 ± 121	304 ± 32	368 ± 129	544 ± 54	577 ± 79	459 ± 30	453 ± 20	394 ± 42	415 ± 26
Fish Swim	466 ± 8	281 ± 77	527 ± 19	473 ± 36	501 ± 11	517 ± 21	587 ± 24	585 ± 23	599 ± 21	596 ± 11
Manipulator Insert Ball	385 ± 12	154 ± 54	409 ± 4	98 ± 29	583 ± 16	625 ± 24	640 ± 26	654 ± 42	631 ± 12	636 ± 43
Manipulator Insert Peg	324 ± 31	71 ± 2	345 ± 12	194 ± 117	384 ± 9	387 ± 36	373 ± 34	365 ± 28	337 ± 23	328 ± 24
Humanoid Run	382 ± 2	1 ± 1	302 ± 6	22 ± 3	586 ± 6	586 ± 6	417 ± 6	412 ± 10	226 ± 7	226 ± 11

Table 6: Results on manipulation environments.

	BC	D4PG	RABM	RCRR exp no-CWP	RCRR exp	RCRR binary no-CWP	RCRR binary	RCRR binary max no-CWP	RCRR binary max
box	166 ± 3	9 ± 9	322 ± 1	340 ± 4	341 ± 4	343 ± 5	351 ± 3	351 ± 4	354.4 ± 4.8
insertion	172 ± 9	0 ± 0	271 ± 3	308 ± 7	316.3 ± 15.0	305 ± 3	312 ± 11	304 ± 13	309 ± 7
slide	91 ± 9	0 ± 0	262 ± 4	314 ± 5	322 ± 11	317 ± 12	325.7 ± 9.4	321 ± 3	322 ± 16
stack banana	230 ± 9	0 ± 0	296 ± 10	320 ± 10	325 ± 7	328 ± 7	341.8 ± 0.7	322 ± 11	328 ± 15

Table 7: Results on locomotion environments.

	BC	D4PG	RABM	RCRR exp no-CWP	RCRR exp	RCRR binary no-CWP	RCRR binary	RCRR binary max no-CWP	RCRR binary max
Humanoid Corridor	220 ± 194	4 ± 4	64 ± 3	902 ± 38	918 ± 14	384 ± 185	484 ± 97	243 ± 146	245 ± 180
Humanoid Gaps	149 ± 9	5 ± 3	94 ± 9	537 ± 55	546 ± 36	152 ± 5	149 ± 89	29 ± 17	33 ± 21
Rodent Gaps	463 ± 137	176 ± 6	420 ± 70	941 ± 17	957 ± 19	485 ± 72	492 ± 117	368 ± 36	392 ± 6
Humanoid Walls	138 ± 77	2 ± 1	131 ± 25	371 ± 17	422 ± 24	294 ± 45	289 ± 72	213 ± 27	232 ± 24
Rodent Escape	388 ± 3	24 ± 14	441 ± 16	420 ± 14	428 ± 26	451 ± 37	444 ± 45	501 ± 29	499 ± 40
Rodent Mazes	343 ± 48	53 ± 1	478 ± 7	471 ± 5	459 ± 7	463 ± 14	464 ± 12	460 ± 18	457 ± 13
Rodent Two Tap	325 ± 60	16 ± 2	598 ± 2	532 ± 32	543 ± 32	615 ± 18	615 ± 19	584 ± 17	588 ± 14